Cross-plane electronic and thermal transport properties of p-type $La_{0.67}Sr_{0.33}MnO_3/LaMnO_3$ perovskite oxide metal/semiconductor superlattices

Pankaj Jha,[1,2] Timothy D. Sands,[1,2,3,a)] Laura Cassels,[4] Philip Jackson,[5] Tela Favaloro,[5] Benjamin Kirk,[6] Joshua Zide,[4] Xianfan Xu,[6] and Ali Shakouri[1,2]
[1]*School of Electrical and Computer Engineering, Purdue University, West Lafayette, Indiana 47907, USA*
[2]*Birck Nanotechnology Center, Purdue University, West Lafayette, Indiana 47907, USA*
[3]*School of Materials Engineering, Purdue University, West Lafayette, Indiana 47907, USA*
[4]*Material Science and Engineering Department, University of Delaware, Newark, Delaware 19716, USA*
[5]*Electrical Engineering Department, University of California, Santa Cruz, California 95064, USA*
[6]*School of Mechanical Engineering and Birck Nanotechnology Center, Purdue University, West Lafayette, Indiana 47907, USA*

(Received 26 March 2012; accepted 24 August 2012; published online 26 September 2012)

Lanthanum strontium manganate ($La_{0.67}Sr_{0.33}MnO_3$, i.e., LSMO)/lanthanum manganate ($LaMnO_3$, i.e., LMO) perovskite oxide metal/semiconductor superlattices were investigated as a potential p-type thermoelectric material. Growth was performed using pulsed laser deposition to achieve epitaxial LSMO (metal)/LMO (p-type semiconductor) superlattices on (100)-strontium titanate (STO) substrates. The magnitude of the in-plane Seebeck coefficient of LSMO thin films ($<20\,\mu$V/K) is consistent with metallic behavior, while LMO thin films were p-type with a room temperature Seebeck coefficient of $140\,\mu$V/K. Thermal conductivity measurements via the photo-acoustic (PA) technique showed that LSMO/LMO superlattices exhibit a room temperature cross-plane thermal conductivity (0.89 W/m·K) that is significantly lower than the thermal conductivity of individual thin films of either LSMO (1.60 W/m·K) or LMO (1.29 W/m·K). The lower thermal conductivity of LSMO/LMO superlattices may help overcome one of the major limitations of oxides as thermoelectrics. In addition to a low cross-plane thermal conductivity, a high *ZT* requires a high power factor ($S^2\sigma$). Cross-plane electrical transport measurements were carried out on cylindrical pillars etched in LSMO/LMO superlattices via inductively coupled plasma reactive ion etching. Cross-plane electrical resistivity data for LSMO/LMO superlattices showed a magnetic phase transition temperature (T_P) or metal-semiconductor transition at ~330 K, which is ~80 K higher than the T_P observed for in-plane resistivity of LSMO, LMO, or LSMO/LMO thin films. The room temperature cross-plane resistivity (ρ_c) was found to be greater than the in-plane resistivity by about three orders of magnitude. The magnitude and temperature dependence of the cross-plane conductivity of LSMO/LMO superlattices suggests the presence of a barrier with the effective barrier height of ~300 meV. Although the magnitude of the cross-plane power factor is too low for thermoelectric applications by a factor of approximately 10^{-4}—in part because the growth conditions chosen for this study yielded relatively high resistivity films—the temperature dependence of the resistivity and the potential for tuning the power factor by engineering strain, oxygen stoichiometry, and electronic band structure suggest that these epitaxial metal/semiconductor superlattices are deserving of further investigation. © *2012 American Institute of Physics*. [http://dx.doi.org/10.1063/1.4754514]

I. INTRODUCTION

Metal/semiconductor superlattices with cross-plane transport offer a novel approach towards improving the thermoelectric materials figure of merit (*ZT*).[1,2] *ZT*, is given by $ZT = \frac{S^2\sigma}{(\kappa_e+\kappa_l)}T$, where *S* is the Seebeck coefficient, σ is the electrical conductivity, κ is the thermal conductivity, and *T* is the absolute temperature (K). The enhancement in ($S^2\sigma$) through energy filtering is possible by engineering the barrier height and cross-plane phonon scattering reduces the lattice contribution to the thermal conductivity.

Existing thermoelectric (TE) materials are restricted in their maximum operating temperature because of low melting or decomposition temperatures, scarce or toxic component elements such as Bi, Te, Co, and Pb, or low *ZT* values at temperatures greater than about 700 K. The thermal and chemical stability of oxides at elevated operating temperatures, the possibility of finding compositions with naturally abundant and nontoxic constituents, and the low production costs for bulk materials make oxides an attractive candidate material for TE devices. Oxides have been previously avoided for TE devices due to strongly ionic behavior and narrow conducting bandwidths from weak orbital overlap leading to localized electrons with low carrier mobilities.[3] However, the prospects for oxides changed when large

a)tsands@purdue.edu.

power factors were observed by Terasaki *et al*. in the magnetic layered cobalt oxide material, $Na_xCo_2O_4$.[4] The power factor is comparable to that of Bi_2Te_3, but the mobility is one order of magnitude lower, suggesting that a low mobility conductor can also be an efficient thermoelectric material. Later, Wang *et al*. proposed that the large power factor in $Na_xCo_2O_4$ is related to its antiferromagnetic behavior at room temperature. The spin states are free to transfer about the crystal and these "moving spins" (spin entropy) carry energy that contributes to the power factor.[5] This unexpectedly large power factor in layered cobalt oxide materials inspired research in p-type materials such as $Ca_3Co_4O_9$ and $Bi_2Sr_3Co_2O_y$. However, *ZT* was found to be low due to high room temperature thermal conductivities (4–5 W/m·K).[6,7] It was later concluded that metal-oxide *ZT* values exceeding 2 would be difficult to achieve because of their large κ_T values (3–10 W/m·K) compared with those of the heavy metallic alloys (0.5–2 W/m·K).[8] While these investigations have attracted a great deal of research, no major breakthroughs in oxide TE materials have yet emerged.

The present study was designed to investigate p-type perovskite oxide metal/semiconductor superlattices as a potential prototype materials system for thermoelectric power generation. Lanthanum strontium manganate $La_{0.67}Sr_{0.33}MnO_3$ (LSMO) was investigated as a metal and lanthanum manganate, $LaMnO_3$ (LMO), as a p-type semiconductor for metal/semiconductor superlattices grown on strontium titanate $SrTiO_3$ (STO) substrates. $La_{0.67}Sr_{0.33}MnO_3$ is based on $LaMnO_3$ (Mn^{3+}, $t^3_{2g}e^1_g$) as the parent compound, where La^{3+} is partially replaced by Sr^{2+}, which forces a partial change of Mn^{3+} to Mn^{4+} with no e_g electron ($t^3_{2g}e^0_g$), resulting in a mixed Mn valence accompanied by hole doping. The hole may hop from a Mn^{4+} ion to a Mn^{3+} ion only if the localized spins are parallel; the hopping action between adjacent Mn ions is dominated by the double-exchange mechanism through an oxygen ion. The double exchange transport mechanism is responsible for the ferromagnetic and conductive ground state for Sr^{2+} doped manganates.[9,10] LSMO is half-metallic, where one spin band is partly occupied at the Fermi level and the other has a nearly zero density of states across the Fermi level.[11] A strontium (Sr) concentration of $x = 0.33$ shows ferromagnetic metallic behavior with a metal work function (Φ_m) of 5.2 eV.[12]

The parent manganese compound $LaMnO_3$ is antiferromagnetic and insulating in its ground state with ion vacancies of La^{3+}, Mn^{3+}, and O^{2-}, which allow doping on all lattice sites. LMO undergoes a structural transformation at $T \sim 523$ K from the Jahn-Teller distorted orthorhombic phase to a high-temperature cubic semiconducting phase.[13] The electrical properties are tunable by varying the oxygen stoichiometry to achieve a p-type semiconductor that conducts by cation transitions. The cation vacancies are responsible for the ferromagnetic as well as the semiconducting behavior.[14] LMO has a band gap of $E_g = 1.1$ eV and electron affinity of 4.4 eV.[15]

The LSMO (metal)/LMO (p-type semiconductor) superlattice is expected to have a Schottky barrier height in the range that would be consistent with effective energy filtering at high temperatures (600–900 K), thereby enhancing the Seebeck coefficient.[16] Based on the relation $\Phi_B = E_g + \chi_s - \Phi_m$, a Schottky barrier ($\Phi_B$) height of ~300 meV at 300 K is expected. LSMO and LMO have closely matched lattice parameters that allow the growth of epitaxial superlattices with sharp interfaces. If the thermal conductivity can be suppressed while enhancing the power factor (increased square of the Seebeck coefficient due to energy filtering that more than offsets the decrease in cross-plane electrical conductivity), then enhanced *ZT* would be expected.[17]

In this paper, the growth of LSMO/LMO superlattices along with characterization of the materials and their electronic and thermal properties is reported. Growth conditions that yield relatively low carrier concentrations have been chosen in order to better isolate relevant physical phenomena in cross-plane thermal and electrical transport by suppressing the effects of parasitic electrical series resistance and the electronic contributions to the thermal conductivity. The results suggest that the barrier height of the superlattice composition investigated is too high for thermoelectric applications near room temperature but possibly suitable for elevated temperature operation. On the other hand, the reduction of lattice thermal conductivity by interfaces is found to be effective, even at room temperature. Finally, the results suggest potential for applications in magnetoresistive sensors at temperatures of 300 K and higher.[18–20]

II. EXPERIMENT

Epitaxial LSMO film growth on (100)-oriented cubic STO substrates was achieved using pulsed laser deposition (PLD) with a 248 nm KrF excimer laser and a pulse width of 25 ns. A laser fluence of 1.3 J/cm^2 and a pulse frequency of 5 Hz were used to ablate the sintered LSMO target. The deposition was performed at a constant substrate temperature of 740 °C, measured using an infrared pyrometer. PLD growth was performed to achieve metallic epitaxial thin films of LSMO on STO using a background O_2 pressure of 50 ± 2 mTorr, which yielded p-type semiconducting LMO. The target was polished prior to each growth to ensure even film growth and to avoid any large particulates breaking off from the roughened target surface due to laser thermal shock or heating of the subsurface before surface vaporization. The LSMO growth rate was 0.13 Å/pulse, with typical film thickness ranging from 300 nm to 400 nm. X-ray diffraction (XRD) 2-theta-omega scans confirmed ⟨001⟩-textured LSMO films on STO substrates without any additional peaks from impurity phases. The rocking curve full-width-at-half-maximum intensity (FWHM) was found to be 0.012°, suggesting an epitaxial film of high crystalline quality. XRD asymmetric 110 Phi scans of LSMO on STO show all four 90°-separated film peaks are well aligned with the substrate peaks, which confirmed highly aligned grains and in-plane epitaxy.

LMO thin-film growth optimization to achieve p-type semiconducting behavior on (100)-STO substrates was also performed using PLD. The laser fluence was maintained at 1.3 J/cm^2 with a pulse frequency of 5 Hz. Variations in oxygen pressure over the range of 40 to 65 mTorr had no impact on the epitaxial growth of the thin films as evaluated by XRD 2-theta-omega scans and Phi scans. In an oxygen pressure window of 45–55 mTorr, a semi-transparent semiconducting thin film of LMO was achieved. The evaporated

target species reacted with the oxygen flow at a pressure maintained at 50 ± 2 mTorr inside the chamber and a substrate temperature of 740 °C to achieve the LMO films with p-type semiconducting behavior. The LMO growth rate was approximately ~0.13 Å/pulse. XRD 2-theta-omega scans confirm c-axis aligned LMO films on STO substrates, and rocking curves of LMO/STO show a small FWHM (0.028°), indicating that the film was of high crystal quality. LMO XRD asymmetric 110 Phi scans confirmed highly aligned grains and in-plane epitaxy.

Finally, p-type LSMO/LMO superlattices were grown on (100)-STO substrates (Fig. 1) using the same growth conditions. XRD 2-theta-omega scans indicate 002 film peaks in the vicinity of the STO 002 peak, and the rocking curves (LSMO FWHM was 0.027° and LMO FWHM was 0.102°) of an LSMO/LMO superlattice were consistent with the anticipated epitaxial relationship (Fig. 2(a)). Asymmetric 110 Phi scans of LSMO/LMO on STO show all four films peaks separated by 90°, confirming in-plane epitaxy for all layers of the superlattice.

In order to determine the degree of relaxation and strain in the superlattice layers, reciprocal space mapping (RSM) of the oxide superlattices was performed. A 110 asymmetric RSM of an LSMO/LMO superlattice is shown in Figure 2(b). In the RSM map, a small degree of spread (low FWHM) and highly intense peaks confirm high-quality pseudomorphic LSMO/LMO superlattice growth on STO substrates. Cross-sectional transmission electron microscopy (TEM) images of the superlattice were taken using an FEI Titan 80–300 operating at 300 kV, revealing the presence of an epitaxial layered structure of high crystalline quality with sharp interfaces and no obvious signs of interlayer diffusion (Fig. 3).

To perform temperature-dependent cross-plane electrical measurements of LSMO/LMO superlattices, cylindrical pillar structures (900 nm height and 300 μm diameter) were fabricated using optically sensitive resist (AZ-9260) as a mask for inductively coupled plasma reactive ion etching (ICP-RIE) (Fig. 4). The optimal etching conditions were 40:10 sccm of Cl_2:Ar, a chamber pressure of 0.7 Pa, an RF forward power of 800 W, and a capacitive bias of 350 W.

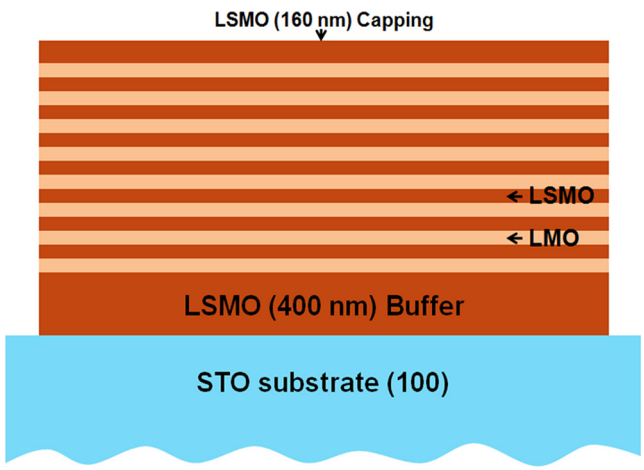

FIG. 1. Schematic of metallic LSMO (8 nm)/semiconducting LMO (8 nm) superlattice $(LSMO/LMO)_{60}$ structure.

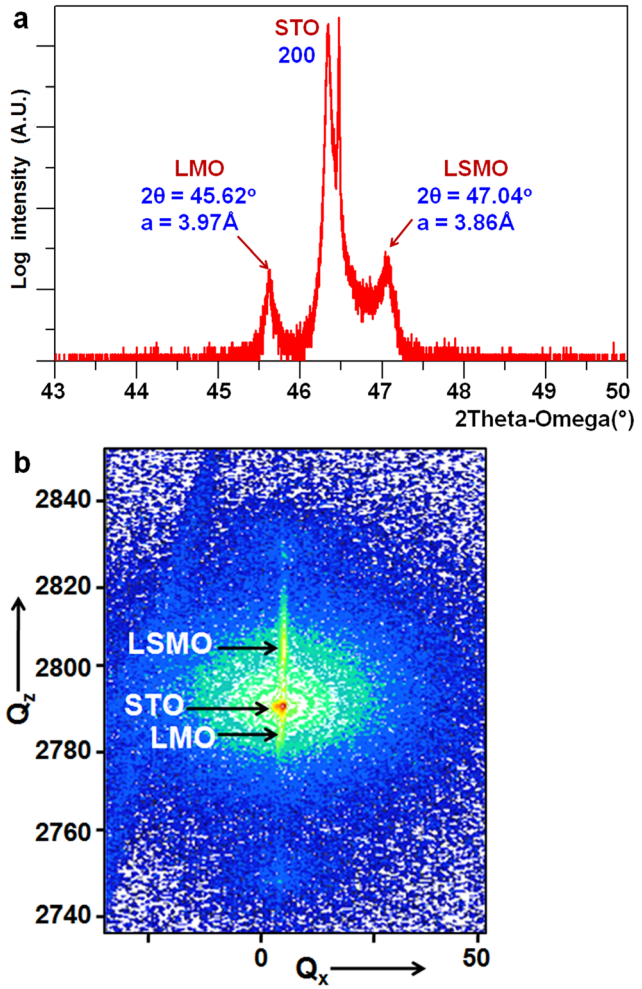

FIG. 2. (a) XRD 2-theta-omega scan of an LSMO/LMO superlattice on a STO (100) substrate confirming c-axis epitaxial behavior with LSMO FWHM (0.027°) and LMO FWHM (0.102°) and (b) 110 RSM of a micron-thick LSMO/LMO superlattice. The LSMO and LMO peaks have a small degree of spread and show a consistent in-plane lattice parameter, confirming the pseudomorphic epitaxial growth of the superlattice film.

The top and bottom contact metallization consisted of three layers, Ti (10 nm)/Pt (40 nm)/Au (500 nm).

III. RESULTS AND DISCUSSION

A. LSMO and LMO thin films

The LSMO and LMO thin films were characterized using Hall effect, four-probe temperature-dependent resistivity (TDR), and in-plane Seebeck measurement techniques. Hall effect characterization of a 400 nm-thick epitaxial LSMO film on STO showed a room temperature resistivity of 0.32 Ω·cm and a hole carrier concentration of 1.38×10^{20} cm^{-3}. In-plane four-probe TDR (Fig. 5(a)) measurements of an LSMO film showed a magnetic phase transition temperature (T_P) or Curie temperature (T_c) at 260 K, accompanied by a metal-semiconductor phase transition, frequently referred to as a metal-insulator transition, which is typically attributed to changes of the spin states, charges, and orbital degrees of freedom.[21] The low temperature ferromagnetic metal to high temperature paramagnetic metal transition causes an increase in conductivity. The transport above the phase transition temperature is governed by the

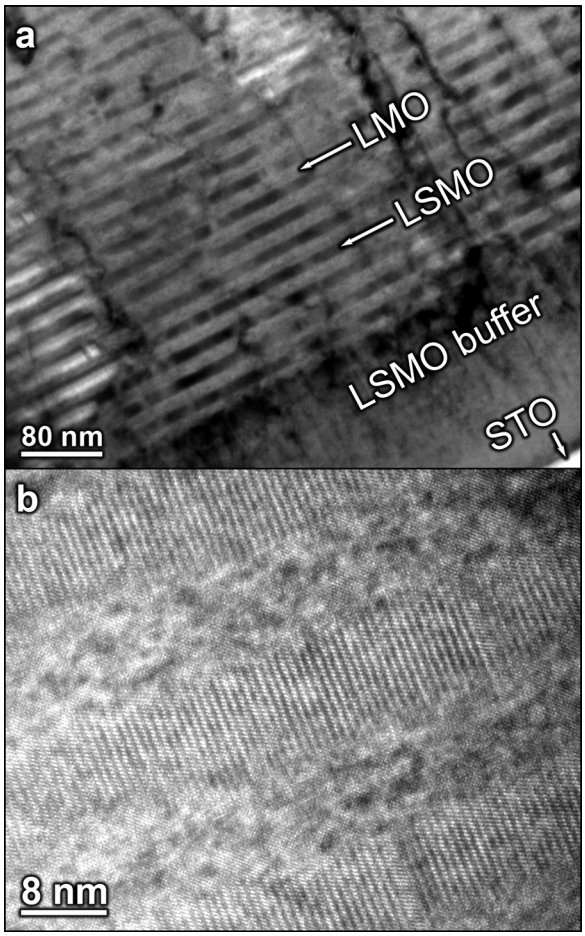

FIG. 3. (a) Low-magnification cross-sectional bright field TEM images of an LSMO (8 nm)/LMO (8 nm) superlattice and (b) high-resolution cross-section TEM confirming epitaxial layer contrast of LSMO/LMO superlattices on a STO (100) substrate were taken using FEI Titan operating at 300 kV. The contrast in (a) along the normal to the growth surface is due to threading dislocations.

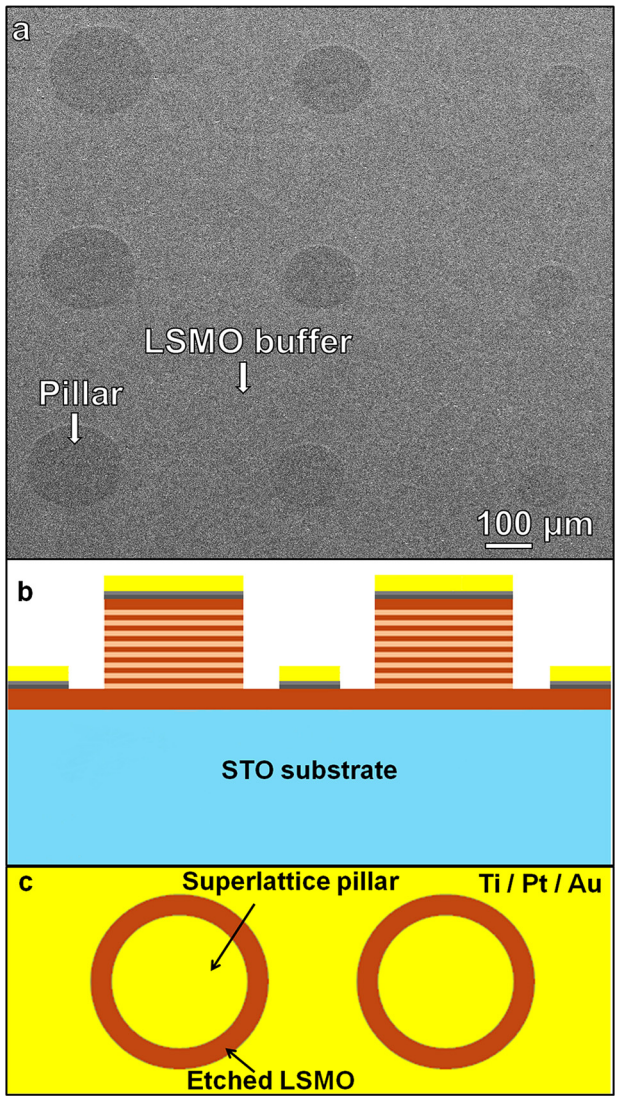

FIG. 4. (a) Top view SEM images of anisotropically etched LSMO/LMO superlattices with pillar heights of 1 μm and the schematic of final structure of LSMO/LMO superlattices for I-V cross-plane measurement. (b) Side view of final structure and (c) top view of final structure.

polaron mechanism[22] yielding a temperature dependence that can be described by a thermal activation energy (E_A) of 162 ± 8 meV, which was extracted using Arrhenius fitting of the temperature dependent conductivity.[23,24] The in-plane Seebeck measurement of LSMO showed a Seebeck coefficient with a magnitude less than 20 μV/K, consistent with metallic behavior (Fig. 6(a)).[25]

Hall effect characterization of a 400 nm epitaxial LMO thin film on STO revealed a room temperature resistivity of 10.4 Ω·cm and a hole carrier concentration of 6.86×10^{18} cm^{-3}. Four-probe in-plane TDR of p-type LMO thin films showed a T_P at 240 K and semiconducting behavior above the phase transition with a thermal activation energy (E_A) of 166 ± 8 meV (Fig. 5(b)). The in-plane Seebeck measurement (Fig. 6(b)) confirmed that the LMO films were p-type with a room temperature Seebeck coefficient of 140 ± 3 μV/K.

Epitaxial LSMO and LMO thin films were also characterized using magnetoresistance (MR) measurements. Magnetoresistance is given by $\Delta R/R_H = (R_H - R_0)/R_H$, where R_0 is the resistance at $H = 0$ T and R_H is measured at 0.2 T. The LSMO in-plane TDR shows a T_P at 260 K and a magnetic field transition (T_{PB}) at 248 K, while the p-type LMO thin films show a T_P at 240 K and a T_{PB} at 220 K (Figs. 5(a) and 5(b)). However, the maximum MR was found to be at temperatures below the T_P and T_{PB} temperatures; LSMO shows an MR ratio of ~16% at 210 K and the LMO MR ratio is ~52% at 200 K, consistent with previous studies of perovskite thin films with magnetic ions on the "B" site.[18–21,26]

B. Thermal conductivity of LSMO/LMO superlattices

Thermal conductivity measurements of LSMO and LMO thin films, as well as p-type LSMO/LMO superlattices, are essential to evaluate potential thermoelectric applications. The room temperature thermal conductivity of thin films and superlattices were measured using the photo-acoustic (PA) technique.[27] The sample was coated with 80 nm of titanium deposited by e-beam evaporation using an Inficon deposition controller to monitor Ti deposition thickness. Each sample and the reference STO bare substrates were coated with Ti simultaneously to achieve the same thickness and tolerance. The sample was heated by the modulated laser beam to generate an acoustic signal. A condenser microphone that was built

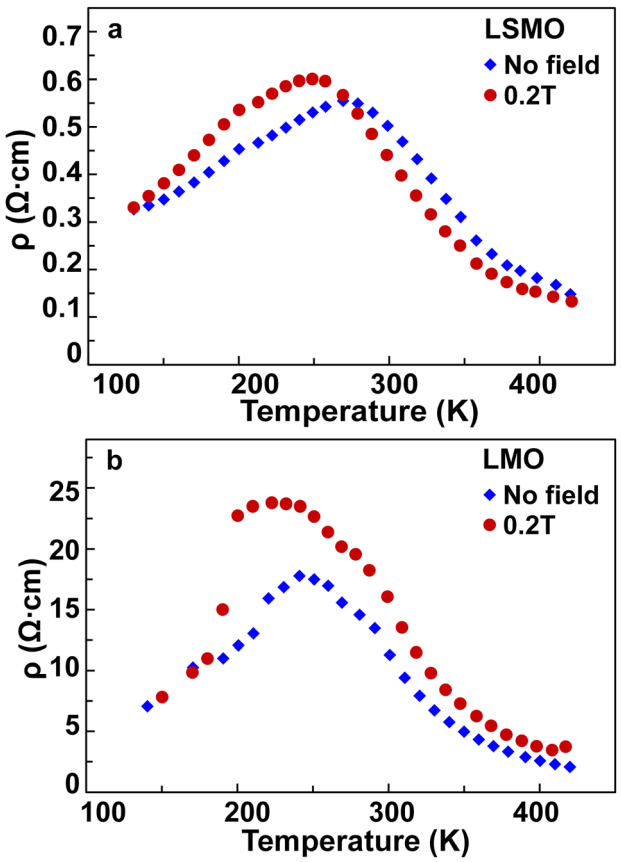

FIG. 5. (a) Temperature-dependent in-plane resistivity of LSMO and (b) temperature-dependent in-plane resistivity of LMO with and without a magnetic field applied in a direction normal to the film surface.

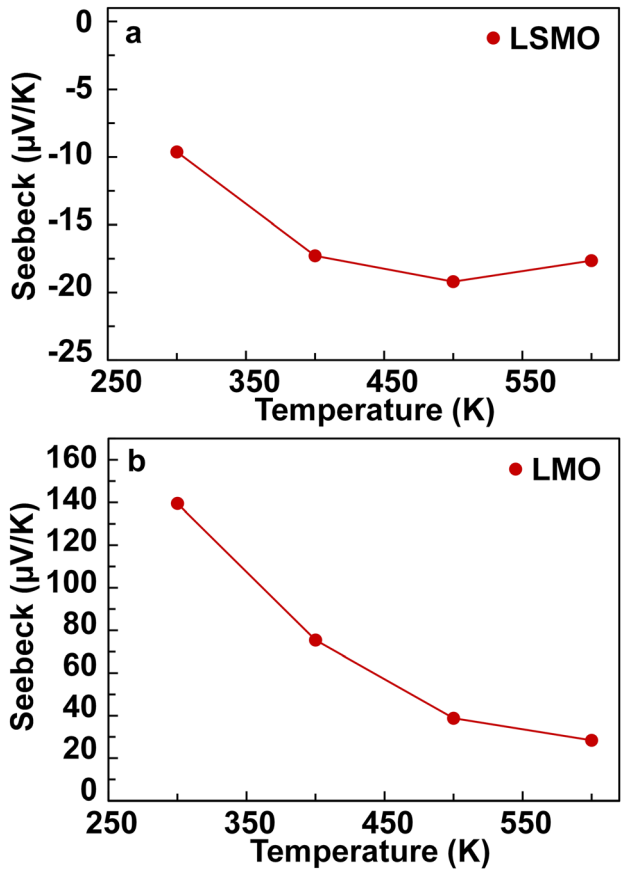

FIG. 6. (a) In-plane Seebeck measurement of LSMO shows Seebeck coefficient consistent with metallic behavior with a magnitude of less than 20 μV/K and (b) in-plane Seebeck measurement of LMO validating p-type behavior with a room temperature Seebeck coefficient of $140 \pm 3\,\mu$V/K.

into the PA cell was used to sense the acoustic signal and transmit to a lock-in amplifier that measured the amplitude and phase shift of the pressure signal. The measured signal was then related to thermal properties of the sample using a heat conduction model.[27] A detailed discussion of the PA measurement technique is available elsewhere.[27,28] The measured cross-plane room temperature thermal conductivities of epitaxial thin films of LSMO and LMO are 1.60 ± 0.075 W/m·K and 1.29 ± 0.025 W/m·K, respectively. Moreover, the cross-plane thermal conductivity of p-type LSMO/LMO superlattices was found to be 0.89 ± 0.21 W/m·K, which is lower than the reported value for bulk oxides, composite materials, or heavy metal alloys. These results indicate that cross-plane phonon scattering reduces the lattice contribution to the thermal conductivity. The experimental amplitude measurements as a function of the modulation frequency are shown for LSMO (Fig. 7(a)), LMO (Fig. 7(b)), and an LSMO/LMO superlattice (Fig. 7(c)). The Wiedemann-Franz law ($\kappa_e = L_o \sigma T$) was used to estimate the electronic contribution (κ_e), where $L_o = 2.44 \times 10^{-8}$ WΩK^{-2}. The lattice contribution to the total thermal conductivity (κ_l) was determined using ($\kappa_l = \kappa_T - \kappa_e$). The electronic contribution to the measured thermal conductivity was found to be negligible. The reduction in thermal conductivity using p-type perovskite LSMO/LMO superlattices suggests that coherent interfaces with nanoscale periods may allow reduction of the lattice thermal conductivity in perovskite oxides to levels that are required for high *ZT* thermoelectric materials.

C. Cross-plane electronic transport in LSMO/LMO superlattices

The in-plane temperature dependent resistivity of epitaxial LSMO/LMO superlattices showed a magnetic phase transition temperature (T_P) of 250 K (Fig. 8(a)) and an extracted thermal activation energy (E_A) of 101 ± 5 meV (Fig. 9). The cross-plane I-V measurement was performed for the p-type LSMO/LMO superlattices as a function of temperature (100–600 K). The extracted cross-plane temperature-dependent resistivity with magnetic phase transition (T_P) or Curie temperature (T_c) at 330 K is shown in Figure 8(b). The apparent T_P was shifted to ~330 K for cross-plane transport through LSMO/LMO superlattices, ~80 K higher than the T_P observed in in-plane measurements of LSMO, LMO or LSMO/LMO thin films. Note, however, that the room temperature cross-plane resistivity (ρ_c) was increased by three orders of magnitude compared to the in-plane resistivity. A similar ρ_c enhancement was reported by Kimura *et al.* with a cross-plane peak shifted downward to 100 K from the in-plane peak at 270 K in a single crystal layered manganate $La_{2-2x}Sr_{1+2x}Mn_2O_7$ ($x = 0.3$).[29–31] Distortion of the LMO octahedron (i.e., MnO_6) and any alteration of the Mn^{4+}/Mn^{3+} ratio, which can be modified by changes in oxygen concentration, have a strong influence on transport properties. Also, tensile strain is responsible for a reduction in T_P based on Jahn-Teller distortion theory.[32,33] We conclude that

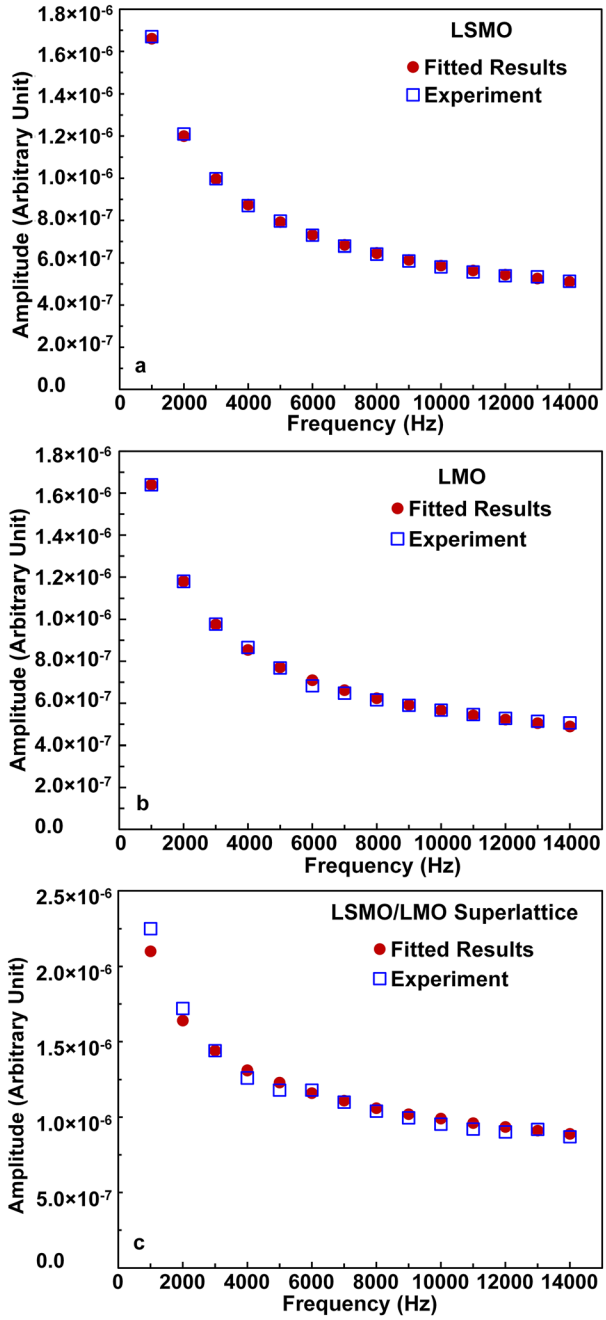

FIG. 7. Photo-acoustic (PA) experimental amplitude measurement as a function of the modulation frequency for (a) LSMO sample, (b) LMO sample, and (c) LSMO/LMO superlattice.

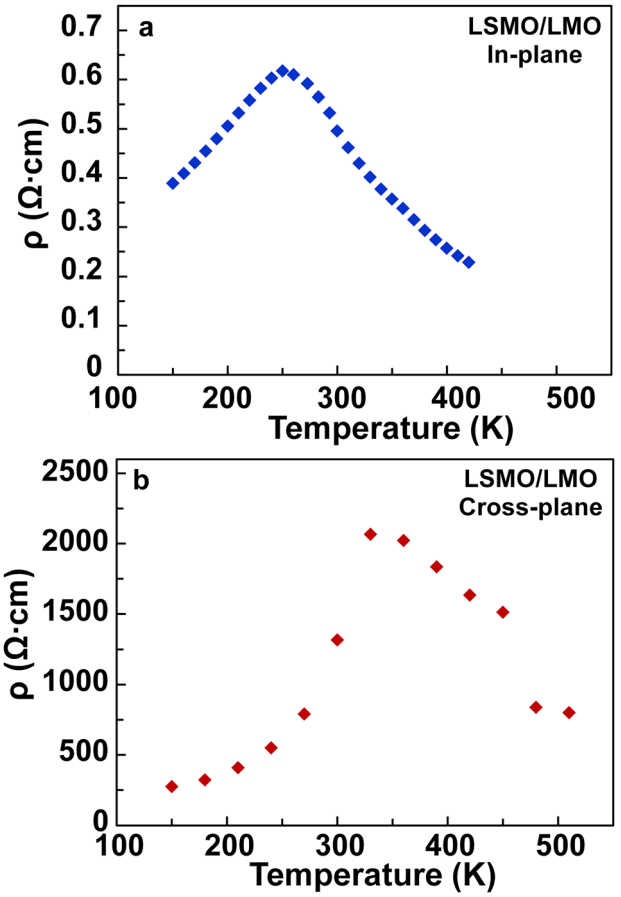

FIG. 8. (a) Measured in-plane resistivity and (b) extracted cross-plane resistivity of p-type LSMO/LMO superlattice using temperature dependent I-V measurement. The magnetic transition peak is shifted to T ~ 330 K in cross-plane transport through LSMO/LMO superlattices, ~80 K higher than the peak observed in in-plane resistivity in LSMO, LMO, or LSMO/LMO thin films.

an increase in the compressive strain of LMO in the superlattice structure enhanced the T_P in the superlattices. This conclusion is supported by an increase in the superlattice LMO FWHM to 0.102°, which is higher than the individual LMO thin film FWHM (0.028°).[34,35] The cross-plane enhancement in T_P around room temperature may be promising for low-magnetic-field magneto-resistive devices, spintronics, field sensors, and magnetoresistive random access memory (MRAM).[24,36]

The extracted cross-plane conductivity of the superlattice structure may suggest a contribution from thermionic behavior above the phase transition temperature. The effective barrier height of 300 ± 15 meV was extracted from the cross-plane temperature-dependent electrical conductivity data from LSMO/LMO superlattices assuming, for simplicity, that the activated process(es) indicated by the temperature dependence was entirely due to thermionic emission over barriers at interfaces (Fig. 10). The extracted experimental barrier height is consistent with the expected LSMO/LMO Schottky

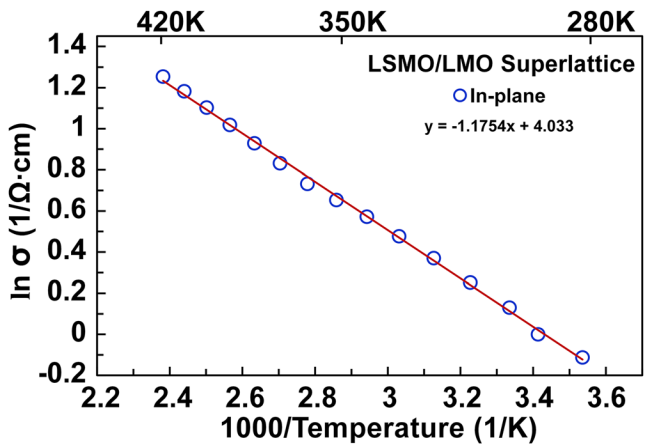

FIG. 9. The in-plane LSMO/LMO superlattices electrical conductivity fitting plot to extract the effective thermal activation energy of 101 ± 5 meV.

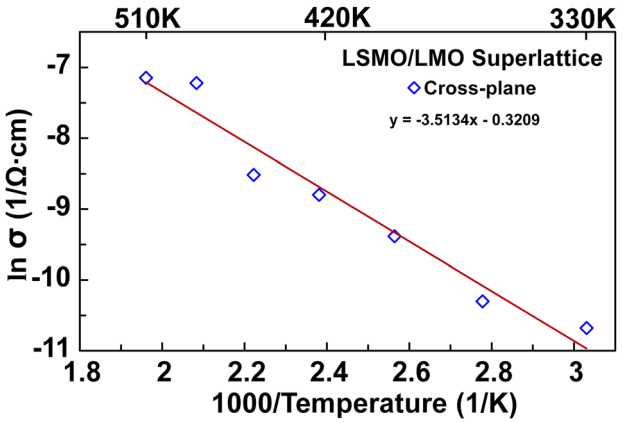

FIG. 10. Arrhenius plot of cross-plane LSMO/LMO superlattice electrical conductivity. The fitting extracted an effective barrier height of 300 ± 15 meV.

barrier (Φ_B) height of ~300 meV at 300 K, which may be responsible in part for a lower than expected cross-plane electrical conductivity at 300 K. That the barrier height is too high for optimal room temperature operation is also supported by a measurement of the cross-plane Seebeck coefficient using a thermal imaging technique.[37] The measured value was 1520 ± 53 μV/K. Combining the cross-plane measurements of the LSMO/LMO superlattices at 300 K yields a *ZT* less than 1×10^{-4}. This low *ZT* is primarily a result of the growth conditions (50 mTorr at 740 °C) chosen for this study. Those conditions yielded films with in-plane resistivities that are more than two orders of magnitude higher than the resistivities obtained at higher oxygen partial pressures during growth.[38] The high resistivities helped to suppress electrical and thermal parasitics in cross-plane transport measurements, thereby simplifying the interpretation of magnetotransport and lattice thermal conductivity measurements. Further measurements at higher temperatures and with lower resistivity heterostructures grown at higher oxygen partial pressures will be necessary to fully evaluate the potential of this oxide superlattice approach.

IV. CONCLUSIONS

Cross-plane transport in LSMO/LMO superlattices has been presented as a potential route to a p-type thermoelectric material. Epitaxial thin-film metallic LSMO and p-type LMO with a room temperature Seebeck coefficient of 140 μV/K were deposited by PLD. The growth parameters of p-type LSMO and LMO were used to obtain high-quality epitaxial, micron-thick LSMO/LMO superlattices, as confirmed by XRD and cross-sectional TEM characterization. The measured cross-plane resistivities of micron-thick LSMO/LMO superlattices show an enhancement of the apparent magnetic phase transition temperature, to $T_P \sim 330$ K, ~80 K higher than either LSMO thin films ($T_P \sim 260$ K), LMO thin films ($T_P \sim 240$ K), or in-plane-measured LSMO/LMO superlattices ($T_P \sim 250$ K). The cross-plane enhancement in T_P and the room temperature cross-plane resistivity increase by three orders of magnitude may be promising for low-magnetic field magneto-resistive devices and MRAM device applications. The room temperature cross-plane thermal conductivity demonstrated in the p-type LSMO/LMO superlattices was 0.89 W/m·K, lower than the cross-plane thermal conductivities of the individual thin-film counterparts (LSMO and LMO). This reduction in lattice thermal conductivity may help to further improve *ZT* in oxide thermoelectrics. Finally, the temperature dependence of the cross-plane electrical resistivity combined with the high value of the cross-plane Seebeck coefficient (1520 μV/K at 300 K) indicate that the barrier height at the LSMO/LMO interface is too high for efficient thermoelectric operation at 300 K. Modification of the barrier height and doping levels for a specific operating temperature range will be necessary to fully evaluate the potential of this approach for thermoelectric devices.

ACKNOWLEDGMENTS

The authors are thankful to Polina Burmistrova for TEM imaging. The authors also like to thank Jeremy Schroeder and Zhixi Bian for their helpful discussions. The authors would like to acknowledge the support by the DARPA Nanostructured Materials for Power program.

[1]A. Shakouri and J. E. Bowers, "Heterostructure integrated thermionic coolers," Appl. Phys. Lett. **71**(9), 1234 (1997).
[2]G. D. Mahan and L. M. Woods, "Multilayer thermionic refrigeration," Phys. Rev. Lett. **80**(18), 4016 (1998).
[3]T. M. Tritt and M. A. Subramanian, "Thermoelectric materials, phenomena, and applications: A bird's eye view," MRS Bull. **31**(3), 188 (2006).
[4]I. Terasaki, Y. Sasago, and K. Uchinokura, "Large thermoelectric power in $NaCo_2O_4$ single crystals," Phys. Rev. B **56**(20), R12685 (1997).
[5]Y. Y. Wang, N. S. Rogado, R. J. Cava, and N. P. Ong, "Spin entropy as the likely source of enhanced thermopower in $Na_xCo_2O_4$," Nature **423**(6938), 425 (2003).
[6]I. Terasaki, "Transport properties and electronic states of the thermoelectric oxide $NaCo_2O_4$," Physica B **328**(1–2), 63 (2003).
[7]I. Terasaki, H. Tanaka, A. Satake, S. Okada, and T. Fujii, "Out-of-plane thermal conductivity of the layered thermoelectric oxide $Bi_{2-x}Pb_xSr_2Co_2O_y$," Phys. Rev. B **70**(21), 214106 (2004).
[8]H. Ohta, S. Kim, Y. Mune, T. Mizoguchi, K. Nomura, S. Ohta, T. Nomura, Y. Nakanishi, Y. Ikuhara, M. Hirano, H. Hosono, and K. Koumoto, "Giant thermoelectric Seebeck coefficient of two-dimensional electron gas in $SrTiO_3$," Nature Mater. **6**(2), 129 (2007).
[9]A. M. Haghiri-Gosnet and J. P. Renard, "CMR manganites: Physics, thin films and devices," J. Phys. D: Appl. Phys. **36**(8), R127 (2003).
[10]C. Zener, "Interaction between the d-shells in the transition metals. 2. Ferromagnetic compounds of manganese with perovskite structure," Phys. Rev. **82**(3), 403 (1951).
[11]G. Banach, R. Tyer, and W. M. Temmerman, "Study of half-metallicity in LSMO," J. Magn. Magn. Mater. **272**, 1963 (2004).
[12]A. Urushibara, Y. Moritomo, T. Arima, A. Asamitsu, G. Kido, and Y. Tokura, "Insulator-metal transition and giant magnetoresistance in $La_{1-x}Sr_xMnO_3$," Phys. Rev. B **51**(20), 14103 (1995).
[13]C. Aruta, M. Angeloni, G. Balestrino, N. G. Boggio, P. G. Medaglia, A. Tebano, B. Davidson, M. Baldini, D. Di Castro, P. Postorino, P. Dore, A. Sidorenko, G. Allodi, and R. De Renzi, "Preparation and characterization of $LaMnO_3$ thin films grown by pulsed laser deposition," J. Appl. Phys. **100**(2), 023910 (2006).
[14]W. S. Choi, Z. Marton, S. Y. Jang, S. J. Moon, B. C. Jeon, J. H. Shin, S. S. A. Seo, T. W. Noh, K. Myung-Whun, H. N. Lee, and Y. S. Lee, "Effects of oxygen-reducing atmosphere annealing on $LaMnO_3$ epitaxial thin films," J. Phys. D: Appl. Phys. **42**(16), 165401 (2009).
[15]T. Kida, G. Q. Guan, and A. Yoshida, "$LaMnO_3$/CdS nanocomposite: A new photocatalyst for hydrogen production from water under visible light irradiation," Chem. Phys. Lett. **371**(5–6), 563 (2003).
[16]D. Vashaee and A. Shakouri, "Improved thermoelectric power factor in metal-based superlattices," Phys. Rev. Lett. **92**(10), 106103 (2004).
[17]R. Venkatasubramanian, "Lattice thermal conductivity reduction and phonon localization-like behavior in superlattice structures," Phys. Rev. B **61**(4), 3091 (2000).

[18]S. Jin, T. H. Tiefel, M. McCormack, R. A. Fastnacht, R. Ramesh, and L. H. Chen, "Thousandfold change in resistivity in magnetoresistive La-Ca-Mn-O films," Science **264**(5157), 413 (1994).
[19]S. Jin, "Colossal magnetoresistance in La-Ca-Mn-O," Met. Mater. **5**(6), 533 (1999).
[20]S. Jin, T. H. Tiefel, M. McCormack, H. Bryan, L. H. Chen, R. Ramesh, and D. Schurig, "Thickness dependence of magnetoresitance in La-Ca-Mn-O epitaxial films," Appl. Phys. Lett. **67**(4), 557 (1995).
[21]M. Imada, A. Fujimori, and Y. Tokura, "Metal-insulator transitions," Rev. Mod. Phys. **70**, 1039 (1998).
[22]J. Millis, P. B. Littlewood, and B. I. Shraiman, "Double exchange alone does not explain the resistivity of $La_{1-x}Sr_xMnO_3$," Phys. Rev. Lett. **74**, 5144 (1995).
[23]M. Ziese and C. Srinitiwarawong, "Polaronic effects on the resistivity of manganite thin films," Phys. Rev. B **58**, 11519–11525 (1998).
[24]H. M. Ronnow, Ch. Renner, G. Aeppli, T. Kimura, and Y. Tokura, "Polarons and confinement of electronic motion to two dimensions in a layered manganite," Nature **440**, 1025 (2006).
[25]T. M. Palstra, A. P. Ramirez, S. W. Cheong, B. R. Zegarski, P. Schiffer, and J. Zaanen, "Transport mechanisms in doped $LaMnO_3$: Evidence for polaron formation," Phys. Rev. B **56**, 5104 (1997).
[26]C. Kwon, K. C. Kim, M. C. Robson, J. Y. Gu, M. Rajeswari, T. Venkatesan, and R. Ramesh, "Desirable magnetotransport properties in doped Mn-oxide-based superlattices," J. Appl. Phys. **81**, 4950 (1997).
[27]H. P. Hu, X. W. Wang, and X. F. Xu, "Generalized theory of the photoacoustic effect in a multilayer material," J. Appl. Phys. **86**(7), 3953 (1999).
[28]X. W. Wang, H. P. Hu, and X. F. Xu, "Photo-acoustic measurement of thermal conductivity of thin films and bulk materials," ASME Trans J. Heat Transfer **123**(1), 138 (2001).
[29]T. Kimura, Y. Tomioka, H. Kuwahara, A. Asamitsu, M. Tamura, and Y. Tokura, "Interplane tunneling magnetoresistance in a layered manganite crystal," Science **274**, 1698 (1996).
[30]Y. Moritomo, A. Asamitsu, H. Kuwahara, and Y. Tokura, "Giant magnetoresistance of manganese oxides with a layered perovskite structure," Nature **380**, 141 (1996).
[31]T. Kimura, Y. Tomioka, A. Asamitsu, and Y. Tokura, "Anisotropic magnetoelastic phenomena in layered manganite crystals: Implication of change in orbital state," Phys. Rev. Lett. **81**, 5920 (1998).
[32]A. J. Millis, T. Darling, and A. Migliori, "Quantifying strain dependence in "colossal" magnetoresistance manganites," J. Appl. Phys. **83**, 1588 (1998).
[33]W. Prellier, M. Rajeswari, T. Ventatesan, and R. L. Greene, "Effects of annealing and strain on $La_{12x}Ca_xMnO_3$ thin films: A phase diagram in the ferromagnetic region," Appl. Phys. Lett. **75**(10), 1446 (1999).
[34]M. Salvato, A. Vecchione, A. De Santis, F. Bobba, and A. M. Cucolo, "Metal-insulator transition temperature enhancement in $La_{0.7}Ca_{0.3}MnO_3$ thin films," J. Appl. Phys. **97**, 103712 (2005).
[35]M. Kanai, H. Tanaka, and T. Kawai, "Origin of metal-insulator transition temperature enhancement in $La_{0.8}Ba_{0.2}MnO_3$ thin films as determined by structural analysis," Phys. Rev. B **70**, 125109 (2004).
[36]S. Yuasa, T. Nagahama, and Y. Suzuki, "Spin-polarized resonant tunneling in magnetic tunnel junctions," Science **297**(5579), 234 (2002).
[37]S. Christofferson and A. Shakouri, "Thermoreflectance based thermal microscope," Rev. Sci. Instrum. **76**(2), 024903 (2005).
[38]M. Huijben, L. W. Martin, Y. H. Chu, M. B. Holcomb, P. Yu, G. Rijnders, D. H. A. Blank, and R. Ramesh, "Critical thickness and orbital ordering in ultrathin $La_{0.7}Sr_{0.3}MnO_3$ films," Phys. Rev. B **78**, 094413 (2008).